IEEE Access
Multidisciplinary | Rapid Review | Open Access Journal

Received 28 May 2023, accepted 5 July 2023, date of publication 11 July 2023, date of current version 19 July 2023.

Digital Object Identifier 10.1109/ACCESS.2023.3294412

APPLIED RESEARCH

Performance Improvement of a Dual-Band Textile Antenna for On-Body Through Artificial Magnetic Conductor

USMAN ALI[1], ABDUL BASIR[2], (Member, IEEE), MUHAMMAD ZADA[2], (Graduate Student Member, IEEE), SADIQ ULLAH[1], (Senior Member, IEEE), BABAR KAMAL[3], AND HYOUNGSUK YOO[2], (Senior Member, IEEE)

[1]Department of Telecommunication Engineering, University of Engineering and TechnologyMardan, Mardan 23200, Pakistan
[2]Department of Electronic Engineering, Hanyang University, Seoul 04763, Republic of Korea
[3]Center of Intelligent Acoustics and Immersive Communications, Northwestern Polytechnical University, Xi'an 710072, China

Corresponding authors: Hyoungsuk Yoo (hsyoo@hanyang.ac.kr) and Sadiq Ullah (sadiqullah@uetmardan.edu.pk)

This work was supported by the Institute for Information and Communications Technology Promotion (IITP) Grant funded by the Korean Government through the Ministry of Science, and Information & Communications Technology (ICT) and Future Planning (MSIP) under Grant 2022-0-00310.

ABSTRACT The increasing demand for wireless communication in wearable devices has led to the need for wearable antennas with a low profile, flexibility, robustness, low SAR, and acceptable on-body performance for WBAN applications. This study presents a low-profile dual-band wearable antenna for WBAN applications operating at 2.45 and 5.8 GHz. The antenna is integrated with a 3×3 artificial magnetic conductor array to reduce backward radiation and improve performance when worn on the human body. It is designed and fabricated on a 2 mm-thick flexible felt substrate with a relative permittivity of 1.3 and loss tangent of 0.044. A 0.17 mm-thick superconductive shieldit material is used as conductive material for the antenna and AMC array. The proposed antenna and AMC array have overall volumes of $0.41\lambda_0 \times 0.45\lambda_0 \times 0.016\lambda_0$ and $0.83\lambda_0 \times 0.83\lambda_0 \times 0.016\lambda_0$, respectively. Results indicate that the AMC structure enhances the antenna's gain, radiation efficiency, and bandwidth. The use of AMC reduced the SAR by greater than 98% for 1 and 10 g of human tissue at 2.45 and 5.8 GHz. The proposed design is suitable for WBAN applications due to its low profile, flexibility, robustness, low SAR, and acceptable on-body antenna gain and bandwidth.

INDEX TERMS Artificial magnetic conductor (AMC), CST MWS, felt, flexibility, Shieldit, wireless body area network (WBAN), wearable antennas.

I. INTRODUCTION

Owing to their application potential in health monitoring, sports, emergency services, entertainment, identification systems, rescue operations, physical training, and security data processing, wireless body area networks (WBANs) have attracted significant attention of the research community and appeared as the interesting topic for researchers [1]. In body wearable applications, the wearer is examined and tracked in real-time with data sent to nearby or distant wearable devices. According to the communication method, these communications are divided into two broad categories, that is, on- and off-body communication [2], [3], [4]. The communication between body-mounted devices is known as on-body communication, while the communication between the base unit and body-worn devices is known as off-body communication. The wearable antennas are the key components of WBANs and play a critical role in such communication because they are responsible for transmitting and receiving signals between wearable devices [5]. Wearable antenna designs are different from traditional antennas, and must have characteristics such as a low profile; flexibility; safety; robustness under

The associate editor coordinating the review of this manuscript and approving it for publication was Hussein Attia.

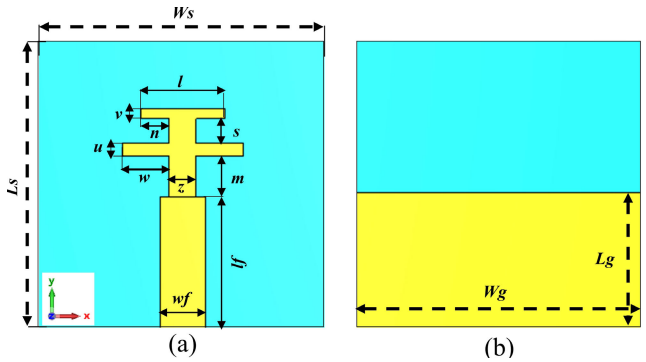

FIGURE 1. Layout of the proposed design (a) front view, (b) back view.

TABLE 1. Summary of the dimensions of the proposed design.

Parameter	Value (mm)	Parameter	Value (mm)
Ls	51.30	*Z*	5.20
Ws	56.12	*S*	4.66
Lg	25.65	*L*	16.40
Wg	56.12	*V*	2.00
Lf	26.65	*N*	5.60
wf	8.97	*U*	2.50
m	8.08	*W*	9.20

stretching, bending, and crumpling scenarios; good radiation characteristics when placed near the human body; low specific absorption rate (SAR), multi-bands; and simple integration into the human body/clothes [6], [7]. Realizing a wearable antenna design that simultaneously satisfies these requirements is difficult [8].

Wearable antennas operate near the human body; hence, the following two main challenges faced by antenna engineers must be carefully studied and addressed. First, as these antennas are placed in intimate contact with the human body, the degree of flexibility of the antenna must be considered. To attain good flexibility, these antennas are designed on flexible/textile material, allowing the antenna to take shape and post the wearer [9], [10], [11]. The flexible materials as substrates that are used for such antennas are textile [12], [13], [14], polyester film [15], paper-based [16], polyimides [17], [18], [19], [20], and latex [21]. In contrast, highly conductive textile materials (e-textiles) are used as flexible materials for the radiating element and ground plane. The commonly used conductive materials are Zelt [22], Flectron [23], Taffeta [24], and Shieldit [25], having electrical conductivities of 1×10^6, 5.88×10^7, 2.5×10^5, and 1.18×10^5 S/m, respectively. Shieldit material, which is plated with copper and nickel and has a surface resistivity of less than 0.05 /Sq., was used in this work. However, the flexibility of the antennas also accompanies with some adverse effects of antennas [25]. For example, wearable antennas reported in the literature are mostly single-band and multiband monopoles and patches. However, their resonant frequency is shifted toward the left or right in bending conditions depending on the geometry of the antennas. To overcome this issue, wideband and ultra-wideband (UWB) wearable antennas have also been reported in [9] and [10]. Nevertheless, wideband antennas encounter issues such as interference. Therefore, an efficient technique is required to isolate narrow and multiband antennas from the effect of the body.

Second, as the antenna operates within the vicinity of the human body, the hazardous radiation is absorbed by human tissue and damages the tissue, which is termed as specific absorption rate (SAR). Thus, the SAR due to the wearable antenna must be considered and should comply with the safety limits specified by the Federal Communication Commission (FCC) and International Commission on Non-Ionizing Radiation Protection (ICNIRP). These standards are 1.6 W/kg for any 1 g of tissue and 2 W/kg for any 10 g of tissue, respectively [26], [27]. The SAR is directly related to the E-field on the human body, which can be minimized by mitigating the back radiations of the antenna towards the human body, and achieves a high front-to-back ratio (FBR) for body-worn antennas [28]. Ideally, an infinite ground plane ensures negligible back radiations, which is not practical and special attention should be given to the overall size of the antenna; the antenna's overall size should be as small as possible [29].

To optimize performance, minimize backward radiation, increase FBR, reduce coupling between lossy human bodies, and lower SAR through various implemented techniques [30], [31]. However, these techniques have certain drawbacks and limitations. Recently, metamaterial (MMT) structures have been extensively used as an artificial ground plane to enhance the overall performance of an antenna, minimize the coupling of the antenna and human body, and reduce the SAR. The application of MMT in the design of wearable antennas is illustrated in [32]. These structures are also called artificial magnetic conductors (AMC), which are usually referred to as electromagnetic bandgap (EBG) surfaces and high impedance surfaces (HISs). The AMC behaves like a reflector, with a reflection bandwidth of +90 to -90 degrees, resulting in a zero-reflection phase and constructive interference with the antenna image current. By integrating AMC as a ground plane, the SAR is reduced and the radiation characteristics of the antenna, such as gain, efficiency, and FBR, are improved [20], [33]. Furthermore, these surfaces reduce the coupling between the antenna and the human body by providing isolation, which reduces frequency detuning [34]. Different kinds of wearable antennas operating in the single band have been reported in [35] and [36]. Similarly, compact size, low profile, and highly directive dual band wearable antennas designed on flexible/textile substrates have been reported in [37] and [38]. Different EBG structures have been used as a ground plane for improving radiation characteristics [15], [39]. Furthermore, to achieve a high FBR by reducing back radiations toward the human body, DGS surfaces are used [40]. Likewise, several AMC

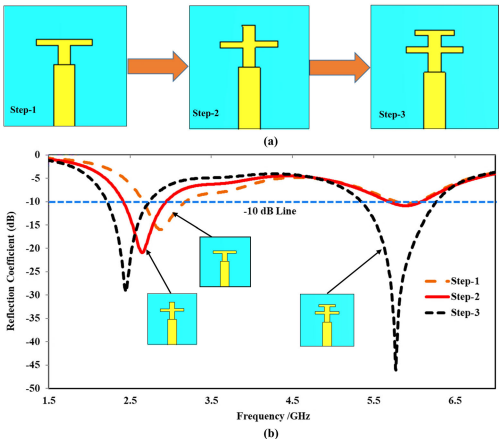

FIGURE 2. Layout and reflection coefficient of the proposed antenna (a) design steps, (b) comparison of the reflection coefficients obtained at various steps.

structures have been proposed for wavefront manipulation and SAR reduction [41], [42]. The antenna systems in the aforementioned studies are inefficient and mostly based on rigid PCBs.

To satisfy the requirements of wearable antennas such as high efficiency, safeguarding antenna's performance from body effects, minimizing the human body from back radiation, and flexible geometry of the antenna, we designed an AMC-based dual-band textile-based antenna operating frequency bands of 2.45 and 5.8 GHz. The proposed antenna is designed and fabricated on a nonconductive material felt with a relative permittivity of 1.3 and a loss tangent of 0.044. To overcome the issues of low gain, frequency detuning, and higher SAR, an AMC structure is used as a ground plane for the proposed antenna. The performance of the antenna with and without the AMC structure is analyzed in terms of gain, radiation efficiency, and driving point impedance under various bending conditions in on- and off-body scenarios. To prove the reliability and robustness of the proposed design, the antenna is fabricated and tested for on- and off-body scenarios. To ensure the safety of the on-body experiences, SAR analysis is also conducted. The design and analysis of the proposed work are performed using the CST MWS full-wave simulation tool. The fabricated antenna is analyzed using Anritsu MS46522A VNA. The stability in the measured results describes the suitability of the proposed antenna for body-worn applications.

II. DESIGN AND CHARACTERIZATION

This section presents the detailed design process of the proposed wearable antenna and MMT. First, the proposed dual-band wearable antenna was designed using the traditional methodology, followed by the design and characterization of the dual-band MMT structure in the proposed frequency bands (2.45 and 5.8 GHz). In the successive section, the integration of the MMT structure with the proposed antenna is reported and on- and off-body analysis results are presented.

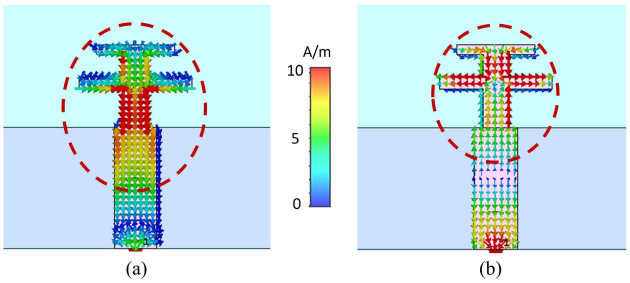

FIGURE 3. Current distribution of the proposed wearable antenna at (a) 2.45 GHz, (b) 5.8 GHz.

A. ANTENNA DESIGN AND PARAMETRIC ANALYSIS

The layout of the proposed dual-band wearable antenna operating at the frequency bands of 2.45 and 5.8 GHz is illustrated in Fig. 1. The design and analysis of the antenna was conducted using the CST MWS full-wave simulation tool. The antenna was designed on a 2-mm-thick felt substrate with a relative permittivity of $\varepsilon_r = 1.3$ and loss tangent of 0.044. A 0.17-mm-thick shielding superconductive material with an estimated conductivity of 1.85×10^5 S/m was used for the radiating element and ground plane. The overall size of the antenna is $0.41\lambda_0 \times 0.45\lambda_0 \times 0.016\lambda_0$. The felt was chosen because it is widely available, inexpensive, and has various sizes. The design of the radiating element consists of a lower T section, a strip, and an upper T section, which generates the low (2.45 GHz) and high frequency (5.8 GHz) bands. Current path distribution was considered as a design technique. The step-by-step procedure to obtain the proposed dual-band design is shown in Fig. 2. When the lower T section was added, a band with an S_{11} level lower than -15 dB, centered at 2.87 GHz with a -10 dB bandwidth of 523 MHz, ranging from 2.66 to 3.18 GHz and a second band around 5.9 GHz with an S_{11} level of -11 dB was obtained. By adding a strip of length 4.66 mm and width of 5.2 mm above the lower T section, the lower band was shifted to 2.64 GHz with an S_{11} level of less than -20 dB, providing a -10 dB bandwidth of 529 MHz, ranging from 2.41 to 2.94 GHz. However, the upper-frequency band remained unchanged. Finally, by adding another T section (upper T), the proposed dual frequency bands were achieved at 2.45 GHz with $S_{11} < -29$ dB, providing a -10 dB bandwidth of 521 MHz, while the second band resonated at a central frequency of 5.8 GHz, and a -10 dB bandwidth of 928 MHz was achieved. The dimensions of the "T" sections within the radiating element of the proposed design were chosen after a parametric study to fine-tune the targeted bands. The summary of the optimized dimensions of the design are listed in Table 1. The antenna was fabricated using an embroidery machine. For the excitation of the fabricated prototype, a 50 Ω standard SMA connector was used.

The current distribution results of the final design at 2.45 and 5.8 GHz are shown in Fig. 3(a) and (b), respectively, which indicates which part of the antenna significantly contributes to making the antenna resonate at the desired

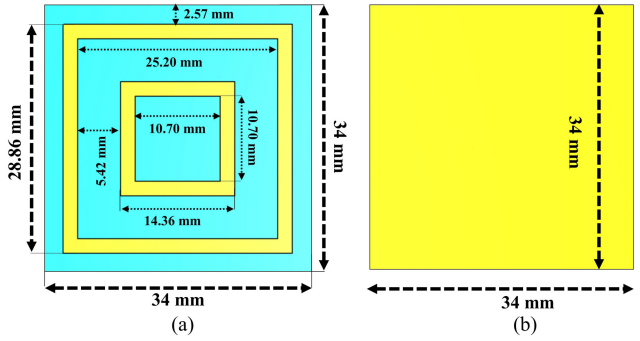

FIGURE 4. Geometry of the proposed AMC unit cell with dimensions (in mm) (a) front view, (b) back view.

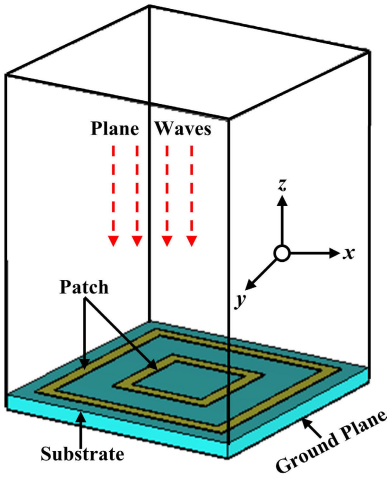

FIGURE 5. Simulation setup for the in-phase reflection characteristic of the proposed unit cell and its geometry.

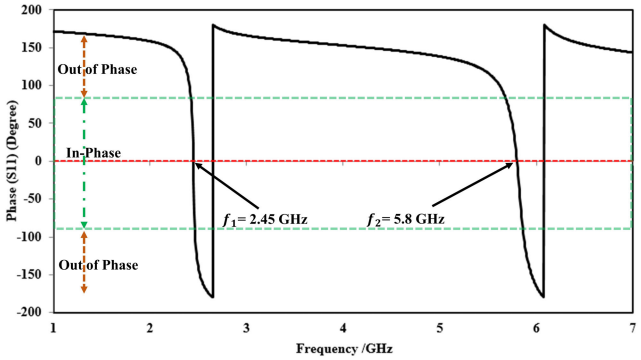

FIGURE 6. Reflection phase characteristic of the proposed dual band AMC structure.

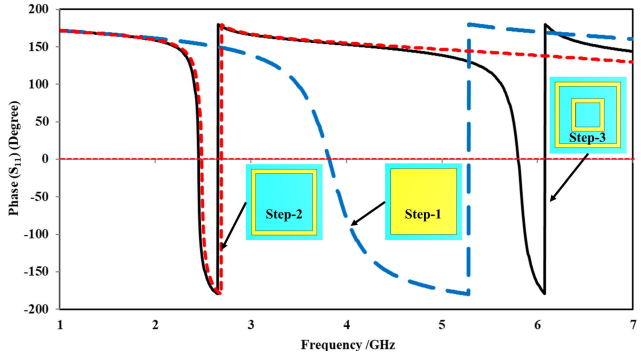

FIGURE 7. Optimization steps of dual-band AMC and their phase response against frequency.

frequency. At the lower frequency band (2.45 GHz), the concentration of the current is around the edge of the lower T section and upper portion of the feedline. While at the higher frequency band (5.8 GHz), it concentrates around the bottom of the feedline, top of the lower T section, the vertical strip between the two T sections, and the lower portion of the upper T sections, which further indicates the radiation mechanism of the antenna at the two frequencies.

B. DESIGN AND CHARACTERIZATION OF AMC STRUCTURE

Considering the applications of wearable antennas, it is essential to reduce the influence of the strong back lobe radiation of the antenna on the human body and to enhance the overall performance of the antenna. An artificial magnetic conductor (AMC) can be used to control the propagation of electromagnetic waves, which makes them suitable to isolate the human body tissue from harmful radiation, enhance gain, and maintain the directional radiation pattern [6], [7]. In this study, an AMC structure was designed and characterized in terms of in-phase reflection. The AMC structure was then integrated with the antenna, and the AMC integrated antenna was analyzed both for on- and off-body scenarios. A simple concentric square ring AMC structure was designed on a 2-mm-thick textile substrate (felt) having a relative permittivity and loss tangent of 1.3 and 0.044, respectively. The AMC top patch and bottom ground plane were built using the highly conductive textile material Shieldit having a conductivity of 1.18 × 105 S/m and thickness of 0.17 mm. The dimensions of the proposed dual-band unit cell were calculated using Sievenpiper's design equations [48]. The total volume of the unit cell was 0.27 λ_0 × 0.27 λ_0 × 0.016 λ_0. The optimized dimension of the proposed unit cell is depicted in Fig. 4. The proposed unit cell was simulated using CST MWS by exciting the surface with a TE10 (linearly polarized) plane wave along the z-axis (from the top). Along the x and y bounds, the criteria were set to the 'unit cell' option. The proposed unit cell's simulation setup for the in-phase reflection characteristic is shown in Fig. 5. Fig. 6 shows the proposed dual-band unit cell's zero-reflection phase at the specified frequencies. The unit cell exhibits a zero-reflection phase at 2.45 and 5.8 GHz to serve as a dual-band reflector for the proposed antenna. The structure behaves exactly like a perfect magnetic conductor (PMC) at these two frequencies [22]. The reflection phases are +180 and −180 degrees at the lower and higher frequencies, respectively. From +180 degrees to +90 degrees and −90 degrees to +180 degrees, the structure acts like a perfect electric conductor (PEC). The reflection phase changes from +90 to −90 degrees, traversing a zero-reflection phase at

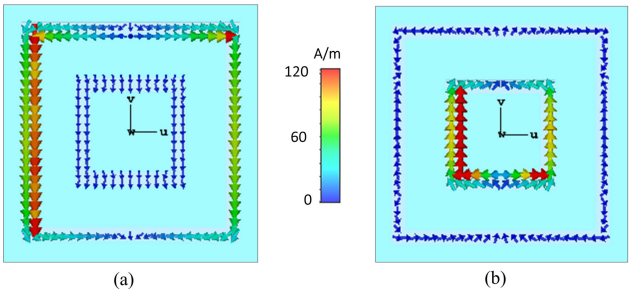

FIGURE 8. Surface current distribution of the proposed AMC unit cell at (a) 2.45 and (b) 5.8 GHz.

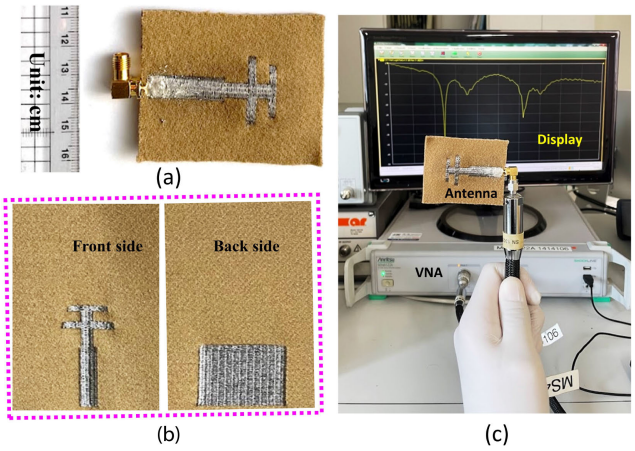

FIGURE 9. Fabricated prototype of the proposed antenna (a) with an SMA connector, (b) front and back view, (c) measured S11 results of the proposed antenna with VNA.

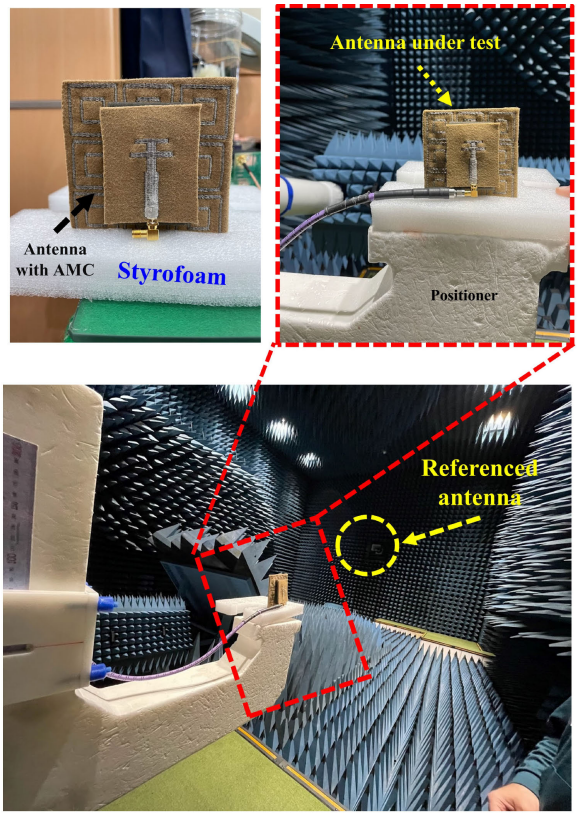

FIGURE 10. Experimentation setup for far-field measurement.

2.45 and 5.8 GHz. The structure behaves like an AMC in this bandwidth. The relationship shown below can be used to determine the reflection bandwidth:

$$BW_{rp} = \frac{f_{(-90)} - f_{(+90)}}{f_c} \times 100 \tag{1}$$

where f_{-90} shows the reflection phase at -90 degrees, and f_{+90} represents the reflection phase at $+90$ degrees. The reflection phase bandwidth obtained from the proposed AMC structure at 2.45 and 5.8 GHz is 4.54% and 10.7%, respectively.

A parametric study of the design procedure of the proposed model was also conducted; the iterative steps in the evolution process are shown in Fig. 7. The design evolution of the proposed unit cell is based on the layout of the typical Mushroom-EBG structure with additional modifications (Fig. 7). In step 1, a simple square patch unit cell was designed, and the unit cell provided a zero-reflection phase at 3.85 GHz. In step 2, a square slot was introduced in the patch to achieve the desired frequency bands. This modification provided a zero-reflection phase at 2.45 GHz. In step 3, an inner square ring was introduced. This modification resulted in a zero-reflection phase at the 2.45 and 5.8 GHz frequency bands. Thus, the proposed unit cell exhibited a zero-reflection phase at two distinct frequency bands to function as a dual-band reflector for the proposed antenna.

In the proposed design, as the dimensions of both squares are different from each other, the capacitance is also different [19]. Therefore, there are two distinct frequencies, which can be determined by the following relationship:

$$f_1 = \frac{1}{2\pi\sqrt{LC_1}} \tag{2}$$

$$f_2 = \frac{1}{2\pi\sqrt{LC_2}}, \tag{3}$$

where f_1, f_2, L, C_1, and C_1 represent the resonant frequencies, inductance, and capacitance of the unit cell.

This observation can be supported by analyzing the surface current distribution of the unit cell at both frequencies, as shown in Fig. 8. The surface current distribution shows that at 2.45 GHz, the outer larger square plays a significant role in this unit cell as a greater amount of current flows over the outer larger square (Fig. 8 (a)). Similarly, at 5.8 GHz, the current distribution is more beyond the inner square (Fig. 8 (b)) than in any other region, which implies that this portion is important in ensuring that this unit cell has a 0° phase at a particular frequency.

III. RESULTS AND DISCUSSION

In this section, the comparison of the simulated and measured results of the proposed wearable antenna with and without an

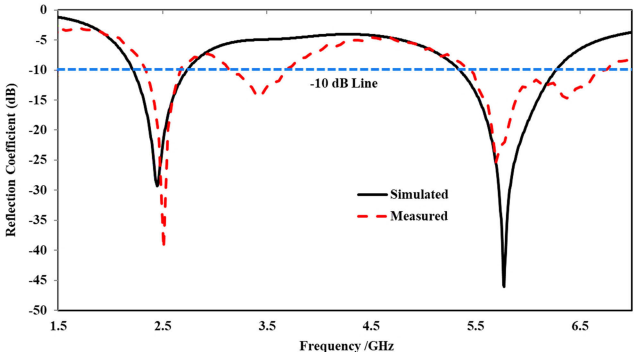

FIGURE 11. Off-body simulated and measured reflection coefficient of the proposed wearable antenna.

TABLE 2. Summary of simulated and measured performance of the proposed antenna.

Parameters	@ 2.45 GHz		@ 5.80 GHz	
	Sim.	Meas.	Sim.	Meas.
Gain (dBi)	2.55	2.49	2.97	3.12
VSWR	1.07	1.12	1.03	1.17
Bandwidth (MHz)	521	418	928	978
Radiation efficiency (%)	87.89	83.29	77.33	79.12

AMC structure in on- and off-body scenarios is presented and explained.

A. OFF-BODY ANALYSIS

In this section, the off-body performance of the proposed wearable antenna is analyzed and compared under flat and bent conditions with and without the AMC structure.

1) ANTENNA PERFORMANCE (FLAT CONDITION)

The proposed antenna was simulated using the CST MWS simulation tool. To validate the results, the antenna was fabricated and tested. The photographs of the fabricated antenna and associated measurement setup at the Applied Bioelectronics Lab (at Hanyang University) for reflection coefficient and far-field measurement are depicted in Figs. 9 and 10, respectively. For the far-field measurement, the proposed antenna was fixed on the positioner in the far-field zone of a broadband horn antenna (probe).

The reflection coefficient of the simulated and measured results of the proposed design are displayed in Fig. 11. The simulated results show that the antenna operates at two distinct frequency bands with a bandwidth computed at S11 ≤ -10 dB, which is 521 and 928 MHz at the 2.45 and 5.8 GHz frequency bands, respectively. The measured results validate that the proposed antenna works at two distinct frequency bands centered at 2.48 and 5.7 GHz with a -10 dB bandwidth of 418 MHz for the first band and 978 MHz for the second band. The simulated results are in good agreement with the measured results. Owing to the fabrication and soldering effects, a marginal shift in both frequencies was observed; however, the entire ISM band was still covered.

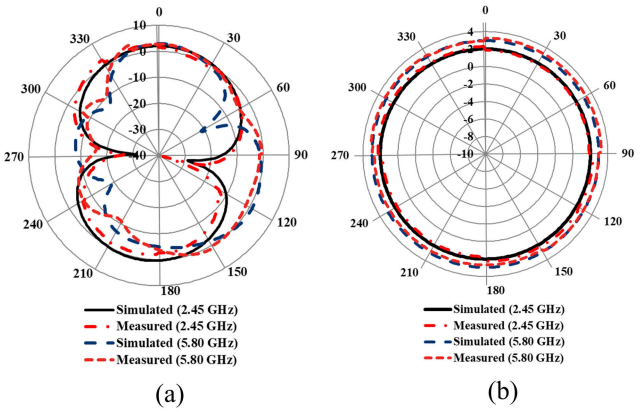

FIGURE 12. Simulated and measured gain comparison of the proposed antenna in (a) *yz*-plane and (b) *xz*-plane.

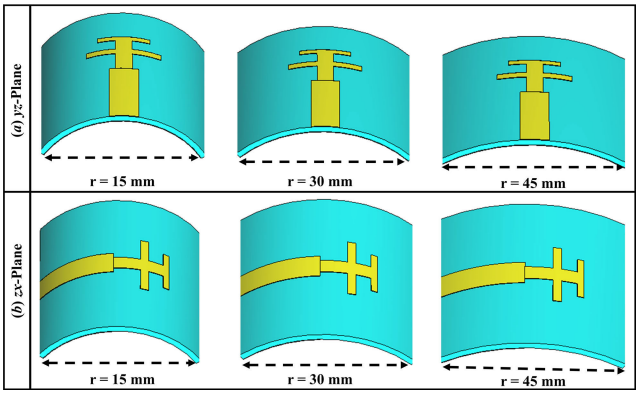

FIGURE 13. Bending analysis of the proposed wearable antenna with various radii in the *xz*- and *xy*-planes.

The far-field characterization of the proposed wearable antenna was analyzed in both the principal planes using the measurement setup shown in Fig. 10. The simulated and measured gain patterns of the proposed wearable antenna in both the E and H planes at the desired frequencies are demonstrated in Fig. 12. The proposed antenna gives a maximum gain of 2.55 dBi and 2.97 dB at 2.45 GHz and 5.8 GHz frequency bands, respectively. In the *yz*-plane, the radiation pattern has a ''figure of eight'' shape, while in the *xz*-plane it provides an omnidirectional radiation pattern. Fig. 12 (a) and (b) show that the patterns are nearly identical, implying that the fabricated prototype gives results that are almost the same as the simulated design. The summary of the simulated and measured performance of the proposed dual-band wearable antenna is summarized in Table 2.

2) ANTENNA PERFORMANCE (BENT CONDITION)

In WBAN applications, wearable antennas can suffer physical deformation due to human body movement. Therefore, it is necessary for wearable antennas to maintain their performances with respect to different deformation. In this

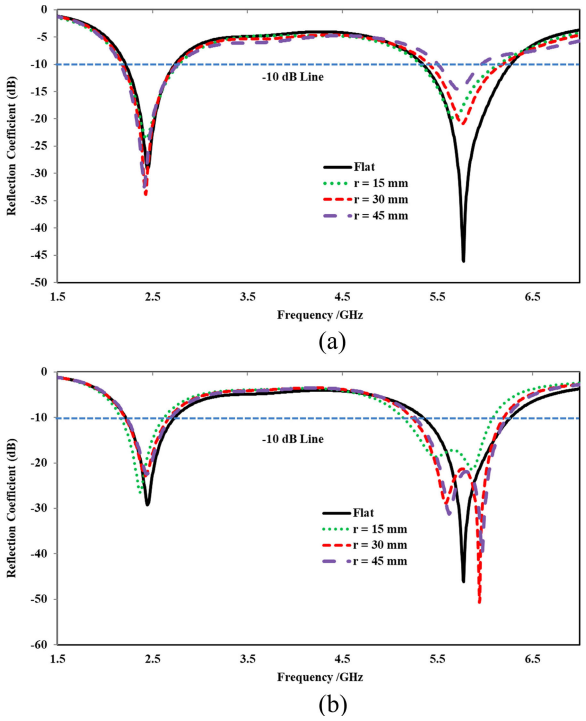

FIGURE 14. Off-body simulated reflection coefficient comparison of the proposed wearable antenna under flat and bent conditions in the (a) *yz*- and (b) *xz*-planes.

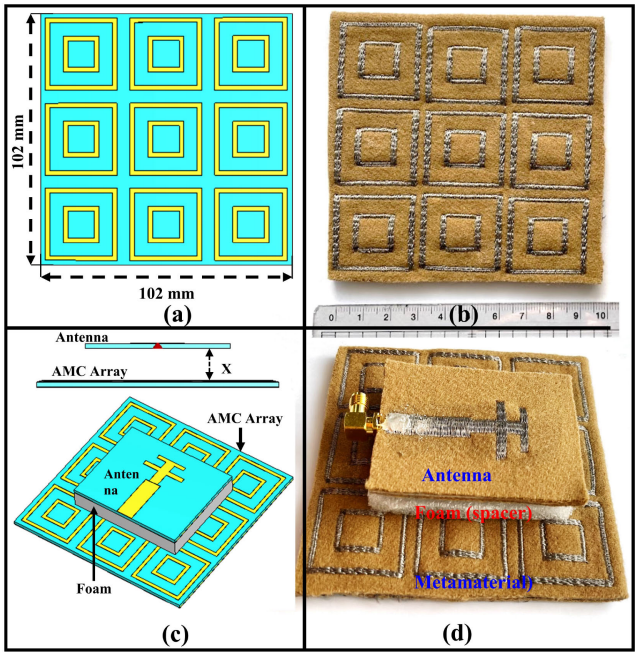

FIGURE 15. Layout of (a) the CST model of the 3 × 3 AMC array and (b) fabricated prototype of the 3 × 3 AMC array; (c) CST model of an antenna without an AMC array; (d) fabricated prototype of an antenna with an AMC array.

section, the effect of bending on the performance of the proposed antenna is demonstrated. The proposed antenna is bent around cylinders of various radii, that is, $r = 15$, 30, and 45 mm in the *xz*- and *xy*-planes (Fig. 13). The off-body simulated reflection coefficients of the proposed antenna in flat and bent scenarios with various radii in the *yz*- and *xz*-planes are presented in Fig. 14. When the antenna is bent along the *yz*-plane, a marginal shift toward the left is observed (Fig. 14(a)) because the effective length of the antenna is reduced. However, the reflection coefficient of the antenna at 2.45 GHz is stable even when it is bent at $r = 45$ mm, while a significant reduction in the reflection coefficient at the 5.8 GHz frequency band is observed relative to the flat antenna. For $r = 15$, 30, and 45 mm, the reflection coefficient was reduced to −17, −21, and −15 dB, respectively, relative to the flat scenario (−35 dB).

Thus, the bending effect along the *yz*-plane is negligible and is considered inconsequential. Similarly, when the antenna was bent along the *xz*-plane, a slight frequency detuning toward the right was observed (Fig. 14(b)); this detuning is due to the decrease in the effective length of the antenna. In addition, a significant reduction in the reflection coefficient at the 5.8 GHz frequency band relative to the flat antenna (−35 dB) was observed for all the bending radii: 15 (−19 dB), 30 (−21 dB) and 45 mm (−22 dB). However, at both the frequency bands, the effect is negligible, and the bandwidth remained stable. In general, regardless of the bending conditions in both principal planes, the performance of the bent antenna was similar to the performance of the antenna in flat conditions, with marginal fluctuation in the reflection coefficient and bandwidth, which implies that the proposed antenna is resistant to bending changes along the *yz*- and *xz*-directions and exhibits satisfactory performance. Thus, the antenna is well-suited for WBAN applications.

3) ANTENNA PERFORMANCE WITH AMC INTEGRATION

The proposed wearable antenna discussed in section A was integrated with a 3 × 3 AMC array, as illustrated in Fig. 15. The total dimension of the 3×3 array was $102 \times 102\ mm^2$. The AMC array structure was placed behind the proposed antenna at a separation of ($X = 3\ mm$) to reduce the electrical contact between the antenna and the AMC array and avoid interaction with the SMA connector [43]. The separation between the antenna and AMC array was realized using a 3*mm*-thicker foam without altering the properties of the AMC integrated antenna. Fig. 15 illustrates the CST model and fabricated prototype of the proposed AMC array and the antenna integrated to the AMC array.

The comparison between the simulated and measured reflection coefficient of the AMC integrated antenna in the off-body scenario is illustrated in Fig. 16. The simulated and measured results were obtained for both the low and high-frequency bands. From the simulated reflection coefficient (solid black), the low band has a center frequency of 2.39 GHz, providing a -10 dB bandwidth of 510 MHz (2.09–2.60 GHz), whereas the high band has a center frequency of 5.8 GHz and exhibits a wider -10 dB bandwidth of 957 MHz (5.36–6.32 GHz). Similarly, according to the

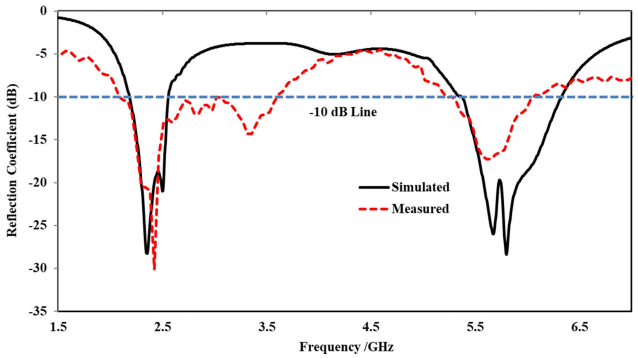

FIGURE 16. Reflection coefficient comparisons of the proposed antenna integrated with AMC.

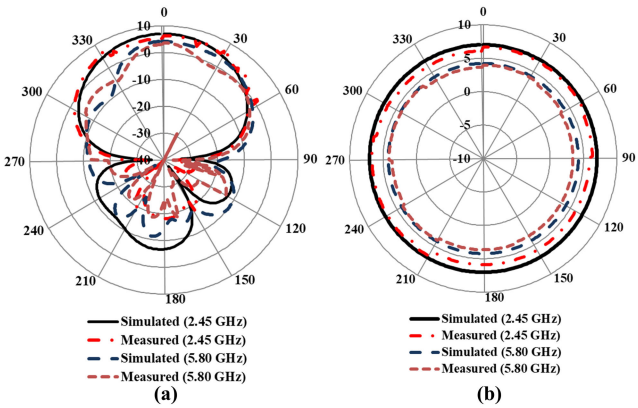

FIGURE 17. Far-field gain comparison of the proposed AMC integrated antenna in both principal planes (a) *yz*-plane and (b) *xz*-plane.

TABLE 3. Simulated and measured performance comparison of the proposed antenna alone and integrated with AMC in off-body conditions.

Parameters	Antenna Alone				Integrated with AMC			
	@ 2.45 GHz		@ 5.80 GHz		@ 2.45 GHz		@ 5.80 GHz	
	Sim.	Meas.	Sim.	Meas.	Sim.	Meas.	Sim.	Meas.
Gain (dBi)	2.55	2.49	2.97	3.12	7.02	6.83	4.23	3.93
Bandwidth (MHz)	521	418	928	978	510	1160	957	900
Radiation efficiency (%)	87.89	83.29	77.33	79.12	91.34	86.12	85.78	83.76

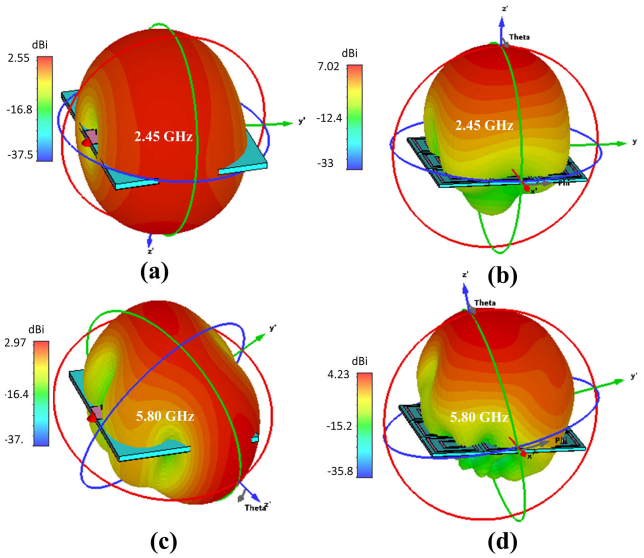

FIGURE 18. Simulated 3D gain patterns of the proposed antenna; (a) and (c) antenna alone; (b) and (d) with AMC.

measured results, the low band (dotted red) has a center frequency of 2.43 GHz; however, it exhibits a wider bandwidth (1.16 GHz), ranging from 2.07 to 3.23 GHz. The high band has a center frequency of 5.68 GHz with a -10 dB bandwidth of 900 MHz, ranging from 5.23 to 6.13 GHz. From Fig. 16, a slight shift can be observed between the simulated and measured results, which is due to several factors, such as the marginal shift observed for an antenna without an AMC structure, as discussed in the previous section (Fig. 11). In addition, it can be a source error or due to the fabrication process or human error. Due to the aforementioned errors and imperfections, the simulated and measured results had a slight deviation from each other; however, the entire ISM band is fully covered, and the antenna can be used for wearable applications.

Fig. 10 shows the far-field measurement setup of the AMC integrated antenna inside the anechoic chamber. Fig. 17 illustrates the far-field simulated and measured gain comparison of the proposed AMC integrated antenna at the desired frequencies. The AMC surface converts the omnidirectional radiation pattern to a directional radiation pattern, thus enhancing the gain of the antenna in both frequency bands. When the AMC surface is integrated with the antenna, the simulated peak gain is increased from 2.55 dBi to 7.02 dBi and 2.97 dBi to 4.23 dBi for the 2.45 and 5.8 GHz frequency bands, respectively. The increase in peak gain is due to the low backward radiation. For further clarification, the 3D gain patterns of the proposed antenna alone and integrated with the AMC at 2.45 and 5.8 GHz were observed and are presented in Fig. 18. This further supports the theory that the increase in gain at both frequencies is due to the transition from an omnidirectional to a directional pattern. The summary of the performance of the proposed antenna with and without the AMC is given in Table 3. The proposed AMC array gives appropriate results at the desired frequencies.

4) MEASUREMENTS OF CONFORMAL AMC-INTEGRATED ANTENNA

All the previous analyses of the antennas were carried out in the flat form; however, in real-world wearable applications, the wearable antennas undergo bending under certain conditions, which can affect the performance of the antenna. Therefore, the performance of the bent antenna integrated with AMC was conducted in measurements in an off-body state. The antenna was bent onto a styrofoam cylinder with diameters of 30, 60, and 90 mm to create various antenna curvatures, which were chosen based on the diameters of

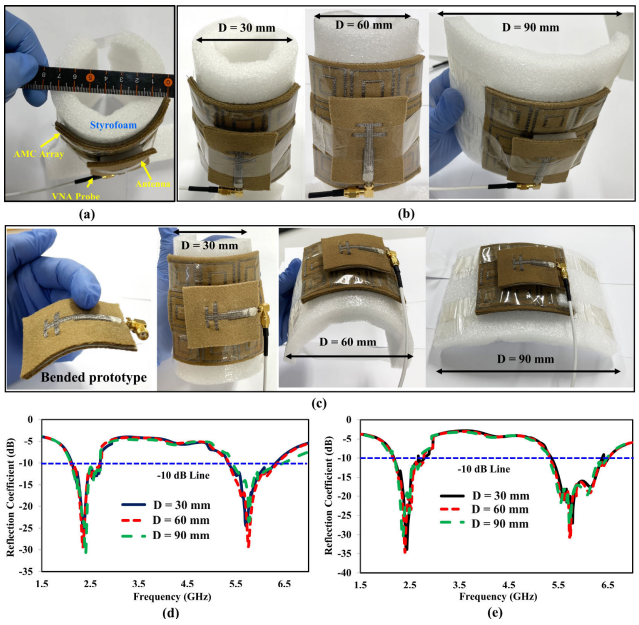

FIGURE 19. Off-body bending analysis of the AMC-integrated antenna at different curvatures with diameters (d) = 30, 60, and 90 mm. (a) Measurement setup for bending analysis. (b) Photographs of bent antennas in yz-plane (E-plane) at diameter (d) = 30, 60, 90 mm. (c) Photographs of bent antennas in xz-plane (H-plane) at diameter (d) = 30, 60, 90 mm. (d) Measured results of the AMC-integrated antenna under bending in E-plane. (e) Measured results of the AMC-integrated antenna under bending in the H-plane.

TABLE 4. Summary of the measured results of the proposed integrated antenna under various bending diameters.

Bending Plane	Diameter	Freq. (GHz)		S_{11} (dB)		Bandwidth (MHz)	
yz	30 mm	2.39	5.72	-25.82	-25.19	336	825
	60 mm	2.41	5.76	-27.94	-29.22	355	862
	90 mm	2.43	5.77	-32.12	-22.34	363	620
xz	30 mm	2.42	5.78	-33.19	-27.22	313	1020
	60 mm	2.40	5.73	-34.43	-31.77	356	1040
	90 mm	2.38	5.71	-30.93	-27.19	363	924

adult leg and arm models. The measured S-parameters of the proposed integrated design with various bending radii in the yz- and xz-planes are illustrated in Fig. 19 (a) and (b), respectively. The results show that the reflection coefficient remained below −25 dB for all bending radii along the yz- and xz-planes. However, the frequency bands (2.45 and 5.80 GHz) slightly shifted to lower frequencies when the antenna was bent at various radii along the yz- and xz-directions. This effect was more significant for extreme degrees of bedding, particularly when $d = 30$ mm in the yz-plane. Conversely, the effect was more significant for a lower degree of bending, particularly when $d = 90$ mm in the xz-plane. A summary of the measured results of the proposed integrated design is presented in Table 4.

TABLE 5. Dielectric characteristics of the human body tissue [46], [47].

Tissue	Permittivity (ε_r)	Conductivity (σ) [S/m]	Permittivity (ε_r)	Conductivity (σ) [S/m]
	@ 2.45 GHz		@ 5.8 GHz	
Skin	38	1.46	35.12	3.71
Fat	5.3	0.11	4.96	0.29
Muscle	52.7	1.77	48.49	4.96

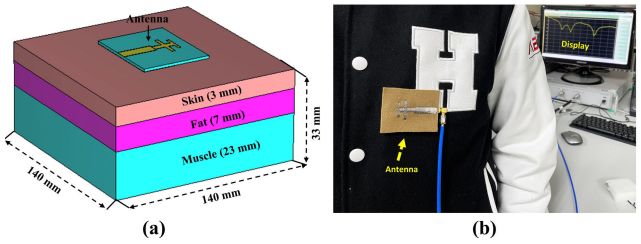

FIGURE 20. Simulated model of the proposed antenna mounted on a three-layer body phantom; (b) Measurement scenario of the proposed antenna on the human body.

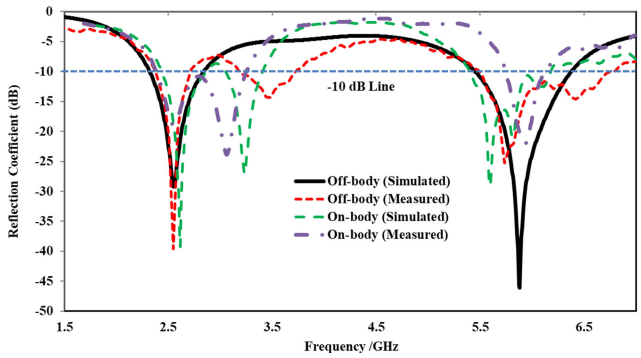

FIGURE 21. On-body and off-body comparison of the simulated and measured reflection coefficients of the proposed antenna.

B. ON-BODY ANALYSIS

Wearable antennas are designed to work in proximity to the human body, and due to the lossy nature and irregularly shaped medium of the human body, the performance of the antenna, such as the radiation pattern, resonant frequency, bandwidth, and particularly the efficiency, is adversely affected [44]. Therefore, for these antennas, the interaction between the human body and the antenna must be considered. Two distinct types of numerical models, namely the theoretical model and the voxel model, known as "phantoms," have been identified and described in the literature [45] to analyze the impact of the human body on the performance of the antenna. After a satisfactory performance of the proposed antenna in the off-body condition, the performance of the proposed antenna must be analyzed near the human body. For this, a three-layer tissue body model mimicking the chest that comprised skin, fat, and muscle layers from top to bottom, as illustrated in Fig. 20 (a), was designed in the commercially

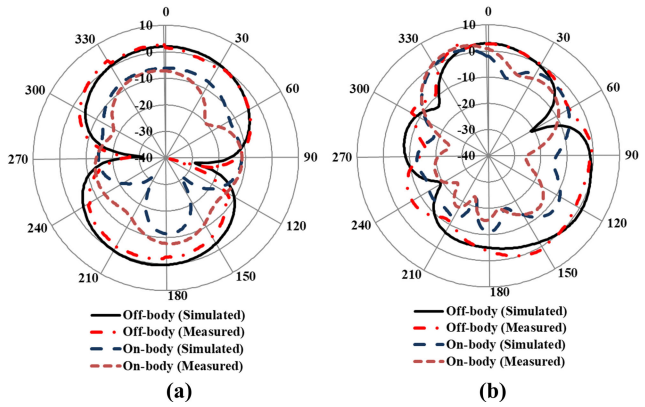

FIGURE 22. On-body radiation pattern gain comparison of the antenna alone in the *yz*-plane at (a) 2.45 and (b) 5.8 GHz.

TABLE 6. Summary of the on-body performance of the proposed antenna alone and integrated with AMC.

Parameters	Antenna Alone				Integrated with AMC			
	@ 2.45 GHz		@ 5.80 GHz		@ 2.45 GHz		@ 5.80 GHz	
	Sim.	Meas.	Sim.	Meas.	Sim.	Meas.	Sim.	Meas.
Gain (dBi)	-6.09	-7.17	1.65	2.64	8.55	7.83	4.31	4.43
Bandwidth (MHz)	326	720	792	425	472	430	1013	1001
Radiation efficiency (%)	45.54	43.55	53.57	55.20	81.83	78.71	73.14	68.18

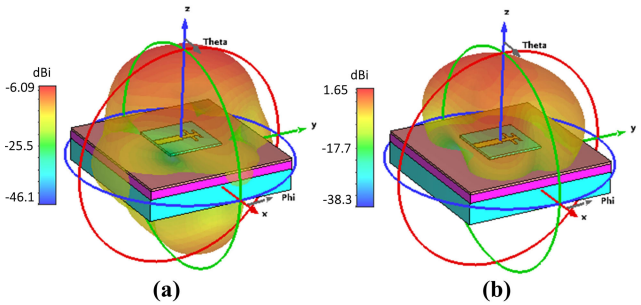

FIGURE 23. On-body simulated 3D gain pattern of the antenna alone at (a) 2.45 and (b) 5.8 GHz.

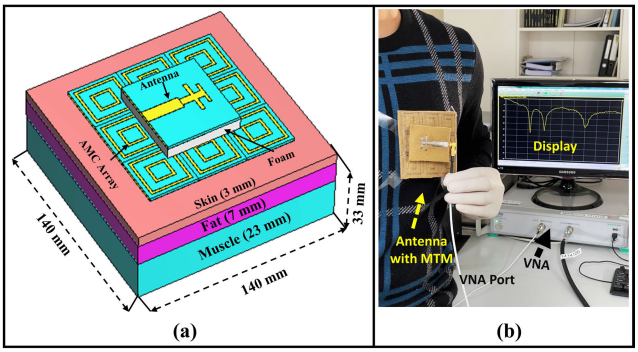

FIGURE 24. On-body analysis of the proposed antenna integrated with AMC. (a) Three-layer human body model (chest) in CST MWS. (b) Fabricated AMC integrated antenna layout placed on the human chest.

available CST MWS software. This 3D numerical model was used to reduce the simulation and processing time. The thicknesses of the skin, fat, and muscle layers were 3, 7, and 23 mm, respectively. The electrical properties of these tissues at two distinct frequencies are given in Table 5. The mass densities (ρ) of the three layers were Skin = 1100 kg/m^3, Fat = 900 kg/m^3, and Muscle = 1060 kg/m^3. The total volume of the phantom was (140 × 140 × 33) mm^3. This section mainly focuses on the on-body analysis and performance evaluation of the proposed antenna alone and integrated with the AMC structure.

1) ANTENNA ALONE

In this section, the performance of the proposed antenna alone is simulated, tested, and analyzed for an on-body scenario. The antenna was placed at a distance (d = 3 mm) above the human body tissue model. In real-world situations, the 3 mm distance represents the cloth and air gap. The prototype of the proposed design was tested by placing it on the human body. The on-body measurement setup of the proposed antenna is illustrated in Fig. 20(b).

The comparison of the simulated and measured reflection coefficient of the proposed antenna for off-body and on-body scenarios is presented in Fig. 21. In contrast to the reflection coefficient in the off-body scenario (standalone condition), the resonant frequency varies in both the low and high-frequency bands in the on-body scenario. There was a shift to the right in the low-frequency band, while the shift was to the left in the high-frequency band. These shifts in both frequency bands are due to the high conductivity and lossy nature of human tissue. At 2.45 GHz, the antenna resonated with a simulated and measured reflection coefficient of (≤-12 dB) with an input impedance of (87 Ω), while at 5.8 GHz, the antenna resonated with a simulated and measured reflection coefficient of (≤-15 dB) and an input impedance of (43 Ω). Additionally, when the antenna was examined for on-body analysis at 2.45 GHz, the measured -10 dB bandwidth rose to 720 MHz, whereas the simulated -10 dB bandwidth dropped from 521 MHz (antenna alone in the off-body state) to 326 MHz. Similarly, the measured impedance bandwidth dropped from 978 MHz (antenna alone in the off-body state) to 425 MHz when the antenna was evaluated for on-body analysis at 5.8 GHz, and the simulated impedance bandwidth dropped from 928 MHz (antenna alone in the off-body state) to 792 MHz (on-body). Fig. 22 presents a comparison of the simulated and measured far-field radiation patterns at the 2.45 and 5.8 GHz frequency bands when the antenna was placed in the proximity of the human body.

Loading the human body deteriorates the radiation pattern and significantly reduces the gain. Radiation efficiency was observed and was compared to the antenna alone in the off-body state, particularly at 2.45 GHz, where the effect is more adverse. The decrease in gain in both the frequency bands, which is one of the primary issues in the wearable antenna design when the antenna is placed in the proximity

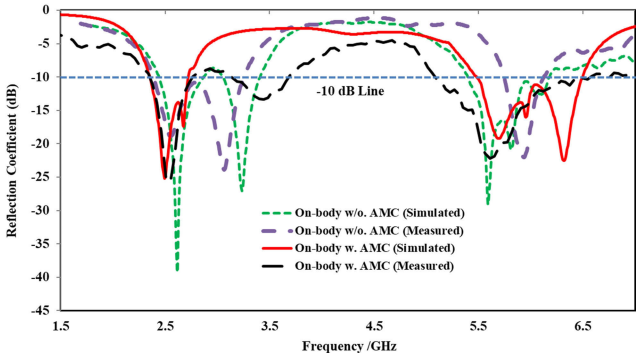

FIGURE 25. Comparison of the on-body simulated and measured reflection coefficient of the AMC integrated antenna.

TABLE 7. Summary of the simulated SAR values of the proposed antenna.

Frequency (GHz)	Antenna Alone		Integrated with AMC	
	SAR (W/Kg)		SAR (W/Kg)	
	1 g	10 g	1 g	10 g
2.45	11.5	5.05	0.138	0.0669
5.80	4.27	1.58	0.0521	0.0322

of the human body, is further justified by the 3D gain pattern illustrated in Fig. 23. Table 6 summarizes the performance evaluation of the proposed antenna alone when placed in proximity of the human body. The analysis shows that when the antenna, which has omnidirectional radiation characteristics, encounters the human body, the majority of the power is consumed in the body, increasing the SAR level above the specified thresholds, which is dangerous and can damage human tissue.

2) ANTENNA INTEGRATED WITH AMC

The main function of the AMC is to isolate the antenna from the adverse effects of the lossy human body, which deteriorate the overall performance of the antenna when placed in close contact. The AMC integrated antenna was evaluated against part of the human body (chest), as shown in Fig. 24(a). The AMC structure was placed in direct contact with the human body, while a separation of 3 mm was maintained between the AMC array and antenna using CST MWS simulation software. The measurement setup for the reflection coefficient of the AMC integrated designs with 3 mm separations of thick foam is depicted in Fig. 24(b). Despite very close contact with human tissue (the chest), the AMC integrated antenna exhibited a stable dual-band resonance that was simulated and was measured to be close to the antenna's reflection coefficient in the off-body scenario. By contrast, without the AMC structure (dashed green and dotted dashed indigo) (Fig. 25), the performance of the antenna was directly influenced by the human body. This demonstrates how the AMC structure affects the performance of the antenna, particularly when placed close to the human

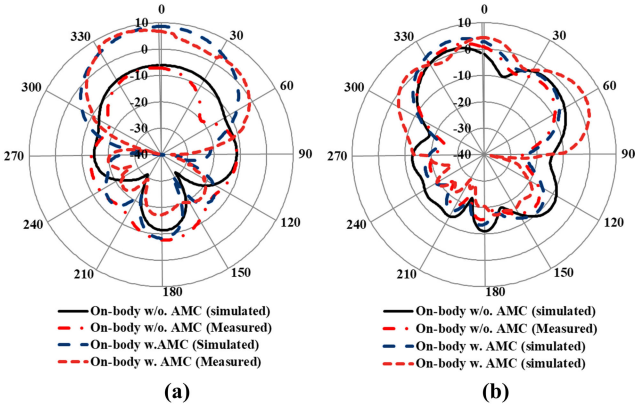

FIGURE 26. On-body radiation pattern gain comparison of the antenna without the AMC and integrated with the AMC at (a) 2.45 and (b) 5.8 GHz.

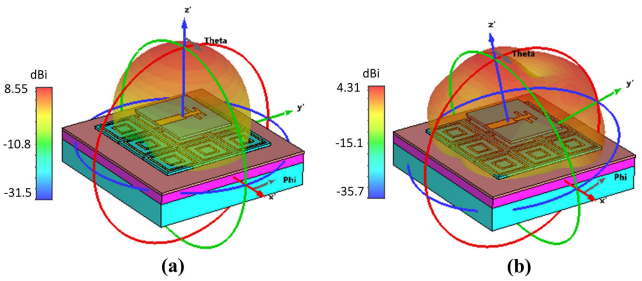

FIGURE 27. On-body simulated 3D gain pattern comparison of the AMC integrated antenna at (a) 2.45 and (b) 5.8 GHz.

body. The AMC integrated antenna on a human body phantom resonated with a simulated and measured reflection coefficient of (≤-16 dB) at 2.45 GHz with a good input impedance of (48 Ω), while at 5.8 GHz, the antenna resonated with a simulated and measured reflection coefficient of (≤-15 dB) with an input impedance of (53 Ω). The antenna also provided adequate bandwidth in both frequency bands. At 2.45 GHz, the measured and simulated -10 dB bandwidths were 472 and 430 MHz, respectively. Similarly, at 5.8 GHz, the measured and simulated impedance bandwidths were 1013 and 1001 MHz, respectively. This implies that the simulated and measured results are in good agreement.

Fig. 26 presents a comparison of the measured and simulated gain of the AMC integrated antenna at the frequency bands of 2.45 and 5.8 GHz when placed near the human body. It is apparent that the maximum gain of the AMC integrated antenna at both frequency bands is higher than that of the antenna without the AMC, for which the gain was severely affected. Fig. 27 depicts the 3D gain pattern, which further demonstrates the increase in gain at both frequency bands. The performance of the proposed AMC integrated antenna when worn on the human body is summarized in Table 6.

IV. SAR ANALYSIS

Wearable antennas operate close to the human body, hence, the SAR value must be calculated. SAR is the energy absorbed by human tissue per unit mass averaged across a

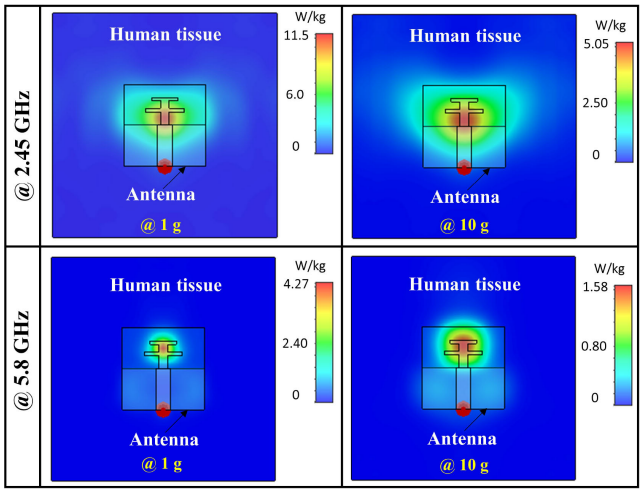

FIGURE 28. Simulated SAR distribution of the proposed antenna alone on three-layer human tissue (Chest).

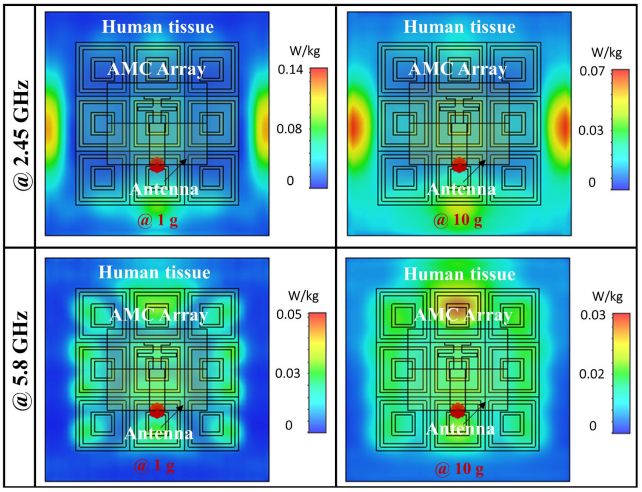

FIGURE 29. Simulated SAR distribution of the proposed antenna with the AMC surface on three-layer human tissue (Chest).

sample volume and is computed in W/kg (typically 1 or 10 g of human body tissue). The value of SAR must not be greater than the limits set by the FCC (1.6 W/kg over 1 g of human body tissue) and ICNIRP (2 W/kg over 10 g of human body tissue) [26]. To verify the safety of the antenna's performance on the human body, the SAR value is simulated using the 1 and 10-g averaging techniques. The SAR of the proposed antenna without AMC and integrated with the AMC structure was evaluated, analyzed, and compared. The antenna alone and integrated with the AMC were simulated using 0.5 W of the input power for both 1 g and 10 g average masses in both frequency bands. As the proposed antenna has omnidirectional radiation characteristics, when it was placed near human tissue, the side and back lobes were directed toward the human body, where they were absorbed and dissipated, increasing the SAR value. The SAR values for the antenna alone were calculated and analyzed to be 11.5 W/kg for 1 g of human tissue and 5.05 W/kg for 10 g of human tissue and 4.27 W/kg for 1 g of human tissue and 1.58 W/kg for 10 g of human tissue at 2.45 and 5.8 GHz, respectively. The 1g of human tissue absorbed more radiation than the 10 g, and the human body was exposed to more radiation at 2.45 GHz than at 5.8 GHz due to the higher conductivity of the human body tissue at 5.8 GHz than that. The SAR level of the proposed antenna at both frequency bands exceeds the safe limits set by the FCC and ICNIRP. Therefore, the SAR level must be within safety limits to ensure user safety, particularly when used in wearable devices for a long time. Incorporating the AMC surface reduced the SAR value to (0.138 W/kg for 1 g of human tissue and 0.0669 W/kg for 10 g of human tissue) and (0.0521 W/kg for 1 g of human body tissue and 0.0322 W/kg for 10 g of human body tissue) at 2.45 GHz and 5.8 GHz, respectively. Hence, the AMC-incorporated antenna complies with both the FCC and ICNIRP standards of safety thresholds and a significant reduction in the SAR value was observed. Therefore, the antenna incorporated with the AMC can be used for WBAN applications. The snapshots of the distribution of the simulated SAR for the antenna without the AMC surface and with it are presented in Figs. 28 and 29, respectively. Table 7 gives an overview of the simulated peak value of the SAR averaged over 1 and 10 g of human tissue.

Table 8 summarizes a comparative study of the proposed dual-band wearable antenna with similar existing work in terms of overall antenna dimensions, type of reflector, number of unit cells used, on-body gain, efficiency, operating bandwidth, SAR, and separation between the human body and antenna. The table shows that the antennas in [2], [20], [48], [49], [54], and [56] have been analyzed and tested at a relatively greater distance from the human body, and hence, these antenna designs are less low profile. Although the antenna in [20] performs satisfactorily, its radiation efficiency is quite low across both frequency bands. Similarly, except for the SAR analysis over 10 g of human body tissue, the antenna described in [48] provides no information on peak gain, operating bandwidth, or radiation efficiency.

Likewise, the design presented in [49] only provides information regarding the SAR analysis for 1 and 10 g of tissue. The antenna presented in [54] is relatively compact and has a wide band; however, its peak gain is low, particularly at 2.45 GHz. In addition, it provides no information on radiation efficiency. The antennas shown in [2] and [56] are constructed on semi-flexible substrates, which means that a high degree of deformation might further impair the overall performance of the antenna. Furthermore, the radiation efficiency of the antenna described in [2] at 2.45 GHz is very poor, and [56] has no information about the radiation efficiency. The antenna presented in [53] has a low bandwidth and efficiency and large dimensions in both frequency bands, which causes discomfort for the users when worn. In addition, the peak SAR at 2.4 GHz is 3.4 W/kg, which is higher than the ICNIRP-approved safe limit. The antennas reported in [34], [50], and [52] are low-profile and offer a reasonably good gain in both frequency bands. However, the antenna

TABLE 8. Comparative study of the proposed work with the state-of-the-art.

Ref.	Antenna size (mm^3)	Substrate/ Flexibility	Operating Frequency (GHz)	Reflector plane/size Array	Distance from body	On-body Efficiency (% age)	Operating Bandwidth (MHz)	Peak SAR (W/kg)	
								1 g	10 g
[2]	$0.23\lambda_o \times 0.15\lambda_o \times 0.01\lambda_o$	Roger 3003C/ Semi Flexible	2.4/5.4	AMC/ $0.15\lambda_o \times 0.15\lambda_o/1\times2$	$0.08\lambda_o$	50/ 72	--	0.19/ 1.18	--
[20]	$0.24\lambda_o \times 0.20\lambda_o \times 0.0004\lambda_o$	Polyimide/ Yes	2.45/5.8	MMT/ $0.19\lambda_o \times 0.19\lambda_o/3\times3$	$0.04\lambda_o$	61.3/ 67.2	210/ 160	1.44/ 0.75	0.81/ 0.28
[34]	$0.24\lambda_o \times 0.18\lambda_o \times 0.004\lambda_o$	Polyimide/ Yes	2.45/5.8	AMC/ $0.16\lambda_o \times 0.16\lambda_o/3\times3$	$0.008\lambda_o$	53/ 70	--	0.35/ 0.39	--
[48]	$0.38\lambda_o \times 0.36\lambda_o \times 0.01\lambda_o$	Felt/ Yes	2.45/5.8	AMC/ $0.16\lambda_o \times 0.16\lambda_o/4\times4$	$0.08\lambda_o$	40	--	--	0.04/ 0.03
[49]	$0.24\lambda_o \times 0.49\lambda_o \times 0.016\lambda_o$	Nora-Dell-CR Fabric/ Yes	2.45/5.8	EBG/ $0.22\lambda_o \times 0.22\lambda_o/3\times4$	$0.05\lambda_o$	--	--	0.09/ 0.04	0.41/ 0.16
[50]	$0.31\lambda_o \times 0.24\lambda_o \times 0.16\lambda_o$	Felt/ Yes	2.45/5.8	AMC/ $0.14\lambda_o \times 0.16\lambda_o/2\times2$	$0.016\lambda_o$	65/ 75	--	0.07/ 0.18	0.05/ 0.09
[51]	$0.21\lambda_o \times 0.69\lambda_o \times 0.016\lambda_o$	Felt/Yes	2.45/5.8	EBG/ $0.16\lambda_o \times 0.16\lambda_o/3\times3$	--	--	--	--	--
[52]	$0.204\lambda_o \times 0.28\lambda_o \times 0.0012\lambda_o$	Polyimide/ Yes	2.45/5.8	AMC/ $0.16\lambda_o \times 0.16\lambda_o/3\times3$	$0.02\lambda_o$	--	--	--	0.02/ 0.01
[53]	$0.42\lambda_o \times 0.44\lambda_o \times 0.024\lambda_o$	Wash Cotton/ Yes	2.4/5.4	EBG/ $0.25\lambda_o \times 0.25\lambda_o/5\times5$	--	-- 67.44	62.9/ 267	--	3.4/ 1.24
[54]	$0.13\lambda_o \times 0.23\lambda_o \times 0.0012\lambda_o$	Polyimide/ Yes	2.45/5.8	MMT/ $0.25\lambda_o \times 0.25\lambda_o/3\times3$	$0.08\lambda_o$	66/ 80	940/ 640	--	1.33/ 1.45
[55]	$0.44\lambda_o \times 0.44\lambda_o \times 0.008\lambda_o$	Felt	2.45/5.8	EBG/ $0.29\lambda_o \times 0.29\lambda_o/3\times3$	--	--	--	0.08/ 0.13	0.04/ 0.09
[56]	$0.21\lambda_o \times 0.204\lambda_o \times 0.012\lambda_o$	RO4350/ Semi Flexible	2.45/5.8	EBG/ $0.14\lambda_o \times 0.14\lambda_o/3\times3$	$0.08\lambda_o$	--	--	0.42/ 0.03	--
This Work	$0.41\lambda_o \times 0.45\lambda_o \times 0.016\lambda_o$	Felt/Yes	2.45/5.8	AMC/ $0.27\lambda_o \times 0.27\lambda_o/3\times3$	$0.02\lambda_o$	81.83/ 73.14	472/ 1013	0.13/ 0.05	0.06/ 0.03

λ_o is the free space wavelength computed at the low-frequency band.

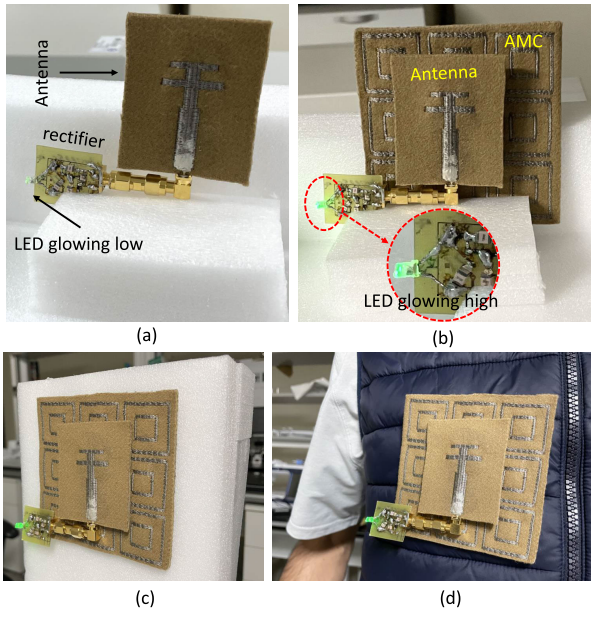

FIGURE 30. Energy harvesting experiments for the proof of concept. (a) Antenna without AMC with rectifier. (b) AMC integrated antenna with rectifier showing LED ON. (c) Off-body energy harvesting. (d) On-body energy harvesting by AMC-integrated antenna.

presented in [50] gives no information regarding the on-body operating bandwidth, while the antennas in [34] and [52] lack details of radiation efficiency and on-body operating bandwidth. Table 8 shows that the proposed design has better gain, efficiency, and bandwidth than that reported in previous works and that it satisfies the ultimate low SAR requirements of the FCC and ICNIRP at both frequency bands. Thus, the proposed antenna is suitable for body-worn wearable applications.

Further, the energy harvesting experiments are carried out as a demo for the proof of concept is shown in Fig. 30. A rectifier circuit, with an LED as a load, is connected to an antenna, which converts the received RF energy to usable DC. The antenna without AMC receives less power as depicted by the low intensity of LED in Fig. 30(a) compared to the AMC-integrated antenna shown in Fig. 30(b). Figs. 30(c) and (d) show the Off-body and On-body energy harvesting capability of the AMC-integrated antenna, respectively.

V. CONCLUSION

This study presents the design and testing of a low-profile, AMC-integrated, wearable dual-band antenna operating at 2.45 and 5.8 GHz in the ISM frequency bands for WBAN applications. The overall size of the antenna was 0.41 λ_0 × 0.45 λ_0 × 0.016 λ_0. At both frequencies, good impedance matching was achieved. The antenna was backed by a 3 × 3 AMC array to limit back radiation and increase the peak gain of the antenna when worn by a human. The dual-band characteristics of the proposed antenna were maintained by this array both in on- and off-body conditions. By incorporating the AMC array, a significant increase in the peak gain and enhancement in the overall performance were achieved at

both the frequency bands in on- and off-body states. Furthermore, as the antenna was designed for wearable applications, the effect of bending the proposed antenna in the *yz* and *xz* directions at different radii were also examined and evaluated. Regardless of the direction of bending and variations in radii, the performance of the antenna remained stable. To ensure the safety of the proposed antenna for WBAN applications, its SAR value was analyzed, and for the AMC integrated antenna, the value of SAR was less than the safety limit established by the FCC and ICNIRP, unlike that in the antenna alone condition. The simulated and measured results were compared, and they were in good agreement. The proposed antenna is well-suited and safe for wearable applications. For future work, further miniaturization of the proposed design, including the AMC reflector, while preserving the overall performance of the antenna is recommended. Moreover, the impact of bending on the SAR of the proposed antenna must also be examined and tested for various human body parts.

ACKNOWLEDGMENT

(Usman Ali, Abdul Basir, and Muhammad Zada are co-first authors.)

REFERENCES

[1] A. Y. I. Ashyap, S. H. B. Dahlan, Z. Z. Abidin, M. I. Abbasi, M. R. Kamarudin, H. A. Majid, M. H. Dahri, M. H. Jamaluddin, and A. Alomainy, "An overview of electromagnetic band-gap integrated wearable antennas," *IEEE Access*, vol. 8, pp. 7641–7658, 2020.

[2] M. A. Shahzad, K. N. Paracha, S. Naseer, S. Ahmad, M. Malik, M. Farhan, A. Ghaffar, M. Hussien, and A. B. Sharif, "An artificial magnetic conductor-backed compact wearable antenna for smart watch IoT applications," *Electronics*, vol. 10, no. 23, p. 2908, Nov. 2021.

[3] H. Zu, B. Wu, P. Yang, W. Li, and J. Liu, "Wideband and high-gain wearable antenna array with specific absorption rate suppression," *Electronics*, vol. 10, no. 17, p. 2056, Aug. 2021.

[4] B. Yeboah-Akowuah, E. T. Tchao, M. Ur-Rehman, M. M. Khan, and S. Ahmad, "Study of a printed split-ring monopole for dual-spectrum communications," *Heliyon*, vol. 7, no. 9, Sep. 2021, Art. no. e07928.

[5] P. S. Hall and Y. Hao, *Antennas and Propagation for Body-Centric Wireless Communications*. Norwood, MA, USA: Artech House, 2012.

[6] A. Badisa, B. T. Madhav, K. Srilatha, M. C. Rao, and S. Das, "A circularly polarized quad-band wearable textile antenna integrated with triple band AMC reflector for WBAN applications," *Prog. Electromagn. Res. C*, vol. 121, pp. 1–18, 2022.

[7] R. Joshi, E. F. N. M. Hussin, P. J. Soh, M. F. Jamlos, H. Lago, A. A. Al-Hadi, and S. K. Podilchak, "Dual-band, dual-sense textile antenna with AMC backing for localization using GPS and WBAN/WLAN," *IEEE Access*, vol. 8, pp. 89468–89478, 2020.

[8] M. M. H. Mahfuz, M. R. Islam, C. Park, E. A. A. Elsheikh, F. M. Suliman, M. H. Habaebi, N. A. Malek, and N. Sakib, "Wearable textile patch antenna: Challenges and future directions," *IEEE Access*, vol. 10, pp. 38406–38427, 2022.

[9] S. Vaezi, P. Rezaei, and A. A. Khazaei, "A miniaturized wideband wearable antenna with circular polarization for medical application," *AEU Int. J. Electron. Commun.*, vol. 150, Jun. 2022, Art. no. 154197.

[10] A. Smida, A. Iqbal, A. J. Alazemi, M. I. Waly, R. Ghayoula, and S. Kim, "Wideband wearable antenna for biomedical telemetry applications," *IEEE Access*, vol. 8, pp. 15687–15694, 2020.

[11] Y.-S. Kim, A. Basir, R. Herbert, J. Kim, H. Yoo, and W.-H. Yeo, "Soft materials, stretchable mechanics, and optimized designs for body-wearable compliant antennas," *ACS Appl. Mater. Interfaces*, vol. 12, no. 2, pp. 3059–3067, Jan. 2020.

[12] X. Lin, Y. Chen, Z. Gong, B. Seet, L. Huang, and Y. Lu, "Ultrawideband textile antenna for wearable microwave medical imaging applications," *IEEE Trans. Antennas Propag.*, vol. 68, no. 6, pp. 4238–4249, Jun. 2020.

[13] B. Almohammed, A. Ismail, and A. Sali, "Electro-textile wearable antennas in wireless body area networks: Materials, antenna design, manufacturing techniques, and human body consideration—A review," *Textile Res. J.*, vol. 91, nos. 5–6, pp. 646–663, Mar. 2021.

[14] S. Agneessens and H. Rogier, "Compact half diamond dual-band textile HMSIW on-body antenna," *IEEE Trans. Antennas Propag.*, vol. 62, no. 5, pp. 2374–2381, May 2014.

[15] B. S. Abirami and E. F. Sundarsingh, "EBG-backed flexible printed Yagi–Uda antenna for on-body communication," *IEEE Trans. Antennas Propag.*, vol. 65, no. 7, pp. 3762–3765, Jul. 2017.

[16] S. Kim, Y. Ren, H. Lee, A. Rida, S. Nikolaou, and M. M. Tentzeris, "Monopole antenna with inkjet-printed EBG array on paper substrate for wearable applications," *IEEE Antennas Wireless Propag. Lett.*, vol. 11, pp. 663–666, 2012.

[17] S. R. Zahran, M. A. Abdalla, and A. Gaafar, "New thin wide-band bracelet-like antenna with low SAR for on-arm WBAN applications," *IET Microw., Antennas Propag.*, vol. 13, no. 8, pp. 1219–1225, Jul. 2019.

[18] S. Genovesi, F. Costa, F. Fanciulli, and A. Monorchio, "Wearable inkjet-printed wideband antenna by using miniaturized AMC for sub-GHz applications," *IEEE Antennas Wireless Propag. Lett.*, vol. 15, pp. 1927–1930, 2016.

[19] M. El Atrash, M. A. Abdalla, and H. M. Elhennawy, "A wearable dual-band low profile high gain low SAR antenna AMC-backed for WBAN applications," *IEEE Trans. Antennas Propag.*, vol. 67, no. 10, pp. 6378–6388, Oct. 2019.

[20] M. Wang, Z. Yang, J. Wu, J. Bao, J. Liu, L. Cai, T. Dang, H. Zheng, and E. Li, "Investigation of SAR reduction using flexible antenna with metamaterial structure in wireless body area network," *IEEE Trans. Antennas Propag.*, vol. 66, no. 6, pp. 3076–3086, Jun. 2018.

[21] K. Agarwal, Y. Guo, and B. Salam, "Wearable AMC backed near-endfire antenna for on-body communications on latex substrate," *IEEE Trans. Compon., Packag., Manuf. Technol.*, vol. 6, no. 3, pp. 346–358, Mar. 2016.

[22] U. Ali, S. Ullah, M. Shafi, S. A. A. Shah, I. A. Shah, and J. A. Flint, "Design and comparative analysis of conventional and metamaterial-based textile antennas for wearable applications," *Int. J. Numer. Modelling, Electron. Netw., Devices Fields*, vol. 32, no. 6, p. 2567, Nov. 2019.

[23] P. J. Soh, G. A. E. Vandenbosch, F. H. Wee, M. Zoinol, A. Abdul, and P. Campus, "Bending investigation of broadband wearable all-textile antennas," *Austral. J. Basic Appl. Sci.*, vol. 7, no. 5, pp. 91–94, 2013.

[24] R. Moro, S. Agneessens, H. Rogier, and M. Bozzi, "Circularly-polarised cavity-backed wearable antenna in SIW technology," *IET Microw., Antennas Propag.*, vol. 12, no. 1, pp. 127–131, 2018.

[25] W. Liu, K. Zhang, J. Li, and S. Yan, "A wearable tri-band half-mode substrate integrated waveguide antenna," *IEEE Antennas Wireless Propag. Lett.*, vol. 20, no. 12, pp. 2501–2505, Dec. 2021.

[26] M. Zada and H. Yoo, "Miniaturized dual band antennas for intra-oral tongue drive system in the ISM bands 433 MHz and 915 MHz: Design, safety, and link budget considerations," *IEEE Trans. Antennas Propag.*, vol. 67, no. 9, pp. 5843–5852, Sep. 2019, doi: 10.1109/TAP.2019.2916585.

[27] A. Yadav, V. K. Singh, P. Yadav, A. K. Beliya, A. K. Bhoi, and P. Barsocchi, "Design of circularly polarized triple-band wearable textile antenna with safe low SAR for human health," *Electronics*, vol. 9, no. 9, p. 1366, Aug. 2020.

[28] M. N. Shakib, M. Moghavvemi, and W. N. L. Binti Wan Mahadi, "Design of a tri-band off-body antenna for WBAN communication," *IEEE Antennas Wireless Propag. Lett.*, vol. 16, pp. 210–213, 2017.

[29] A. Michel, R. Colella, G. A. Casula, P. Nepa, L. Catarinucci, G. Montisci, G. Mazzarella, and G. Manara, "Design considerations on the placement of a wearable UHF-RFID PIFA on a compact ground plane," *IEEE Trans. Antennas Propag.*, vol. 66, no. 6, pp. 3142–3147, Jun. 2018.

[30] K. H. Chan, K. M. Chow, L. C. Fung, and S. W. Leung, "Effects of using conductive materials for SAR reduction in mobile phones," *Microw. Opt. Technol. Lett.*, vol. 44, no. 2, pp. 140–144, Jan. 2005.

[31] M. Haridim, "Use of rod reflectors for SAR reduction in human head," *IEEE Trans. Electromagn. Compat.*, vol. 58, no. 1, pp. 40–46, Feb. 2016.

[32] K. Zhang, P. J. Soh, and S. Yan, "Meta-wearable antennas—A review of metamaterial based antennas in wireless body area networks," *Materials*, vol. 14, no. 1, p. 149, Dec. 2020.

[33] M. A. Abdelghany, M. Fathy Abo Sree, A. Desai, and A. A. Ibrahim, "Gain improvement of a dual-band CPW monopole antenna for sub-6 GHz 5G applications using AMC structures," *Electronics*, vol. 11, no. 14, p. 2211, Jul. 2022.

[34] K. Zhang, G. A. E. Vandenbosch, and S. Yan, "A novel design approach for compact wearable antennas based on metasurfaces," *IEEE Trans. Biomed. Circuits Syst.*, vol. 14, no. 4, pp. 918–927, Aug. 2020.

[35] A. Arif, M. Zubair, M. Ali, M. U. Khan, and M. Q. Mehmood, "A compact, low-profile fractal antenna for wearable on-body WBAN applications," *IEEE Antennas Wireless Propag. Lett.*, vol. 18, no. 5, pp. 981–985, May 2019.

[36] M. Kokolia and Z. Raida, "Textile-integrated microwave components based on artificial magnetic conductor," *Int. J. Numer. Modelling, Electron. Netw., Devices Fields*, vol. 34, no. 4, Jul. 2021.

[37] H. Yang, X. Liu, Y. Fan, and L. Xiong, "Dual-band textile antenna with dual circular polarizations using polarization rotation AMC for off-body communications," *IEEE Trans. Antennas Propag.*, vol. 70, no. 6, pp. 4189–4199, Jun. 2022.

[38] M. N. Ramli, P. J. Soh, M. F. Jamlos, H. Lago, N. M. Aziz, and A. A. Al-Hadi, "Dual-band wearable fluidic antenna with metasurface embedded in a PDMS substrate," *Appl. Phys. A, Solids Surf.*, vol. 123, no. 2, p. 149, Feb. 2017.

[39] S. Velan, E. F. Sundarsingh, M. Kanagasabai, A. K. Sarma, C. Raviteja, R. Sivasamy, and J. K. Pakkathillam, "Dual-band EBG integrated monopole antenna deploying fractal geometry for wearable applications," *IEEE Antennas Wireless Propag. Lett.*, vol. 14, pp. 249–252, 2015.

[40] R. Mondal, P. S. Reddy, D. C. Sarkar, and P. P. Sarkar, "Compact ultra-wideband antenna: Improvement of gain and FBR across the entire bandwidth using FSS," *IET Microw., Antennas Propag.*, vol. 14, no. 1, pp. 66–74, Jan. 2020.

[41] H. Yalduz, T. E. Tabaru, V. T. Kilic, and M. Turkmen, "Design and analysis of low profile and low SAR full-textile UWB wearable antenna with metamaterial for WBAN applications," *AEU Int. J. Electron. Commun.*, vol. 126, Nov. 2020, Art. no. 153465.

[42] Y. Gong, S. Yang, B. Li, Y. Chen, F. Tong, and C. Yu, "Multi-band and high gain antenna using AMC ground characterized with four zero-phases of reflection coefficient," *IEEE Access*, vol. 8, pp. 171457–171468, 2020.

[43] A. Y. I. Ashyap, Z. Zainal Abidin, S. H. Dahlan, H. A. Majid, S. M. Shah, M. R. Kamarudin, and A. Alomainy, "Compact and low-profile textile EBG-based antenna for wearable medical applications," *IEEE Antennas Wireless Propag. Lett.*, vol. 16, pp. 2550–2553, 2017.

[44] A. Mersani, L. Osman, and J. Ribero, "Performance of dual-band AMC antenna for wireless local area network applications," *IET Microw., Antennas Propag.*, vol. 12, no. 6, pp. 872–878, May 2018.

[45] G. Christina, "Review on wearable antennas and their applications," *IRO J. Sustain. Wireless Syst.*, vol. 3, no. 4, pp. 259–265, 2022.

[46] H. Savci, H. Sajjad, S. Khan, and F. Kaburcuk, "Analysis of a compact multi-band textile antenna for WBAN and WLAN applications," *Balkan J. Electr. Comput. Eng.*, vol. 9, no. 3, pp. 255–260, Jul. 2021.

[47] X. Zhu, Y. Guo, and W. Wu, "Miniaturized dual-band and dual-polarized antenna for MBAN applications," *IEEE Trans. Antennas Propag.*, vol. 64, no. 7, pp. 2805–2814, Jul. 2016.

[48] S. Yan, P. J. Soh, and G. A. E. Vandenbosch, "Low-profile dual-band textile antenna with artificial magnetic conductor plane," *IEEE Trans. Antennas Propag.*, vol. 62, no. 12, pp. 6487–6490, Dec. 2014.

[49] G. Gao, B. Hu, S. Wang, and C. Yang, "Wearable planar inverted-F antenna with stable characteristic and low specific absorption rate," *Microw. Opt. Technol. Lett.*, vol. 60, no. 4, pp. 876–882, Apr. 2018.

[50] W. Bouamra, I. Sfar, A. Mersani, L. Osman, and J. M. Ribero, "Dual-band textile AMC antenna for WLAN/WBAN applications on the human arm," *Int. J. Electron. Telecommun.*, vol. 68, no. 2, pp. 209–216, 2022.

[51] M. Mantash, A. C. Tarot, S. Collardey, and K. Mahdjoubi, "Design methodology for wearable antenna on artificial magnetic conductor using stretch conductive fabric," *Electron. Lett.*, vol. 52, no. 2, pp. 95–96, Jan. 2016.

[52] B. Yin, M. Ye, Y. Yu, and J. Gu, "A dual-band, miniaturized, AMC-based wearable antenna for health monitoring applications," *Prog. Electromagn. Res. C*, vol. 112, pp. 165–177, 2021.

[53] A. Wajid, A. Ahmad, S. Ullah, D.-Y. Choi, and F. U. Islam, "Performance analysis of wearable dual-band patch antenna based on EBG and SRR surfaces," *Sensors*, vol. 22, no. 14, p. 5208, Jul. 2022.

[54] H. Zheng, W. Cui, R. Liu, Z. Li, C. Fan, M. Wang, and E. Li, "Design of flexible dual-band antenna and metamaterial structure for wearable body area network," *Int. J. RF Microw. Comput.-Aided Eng.*, vol. 32, no. 5, May 2022, Art. no. e23083.

[55] S. Zhu and R. Langley, "Dual-band wearable textile antenna on an EBG substrate," *IEEE Trans. Antennas Propag.*, vol. 57, no. 4, pp. 926–935, Apr. 2009.

[56] R. Li, C. Wu, X. Sun, Y. Zhao, and W. Luo, "An EBG-based triple-band wearable antenna for WBAN applications," *Micromachines*, vol. 13, no. 11, p. 1938, Nov. 2022.

USMAN ALI received the B.Sc. and M.Sc. degrees in telecommunication engineering from the University of Engineering and Technology (UET) Peshawar, Pakistan, in 2012 and 2017, respectively, where he is currently pursuing the Ph.D. degree in telecommunication engineering. He is a Lecturer with the Department of Telecommunication Engineering, UET, Mardan, Pakistan. His research interests include wearable antennas, SAR analysis, 5G antennas, millimeters wave antennas, reconfigurable antennas, metamaterials, and electromagnetic bandgap structures.

ABDUL BASIR (Member, IEEE) was born in Khyber Pakhtunkhwa, Pakistan, in 1989. He received the B.Sc. degree in telecommunication engineering from the University of Engineering and Technology, Peshawar, Pakistan, in 2015, and the Ph.D. degree in electronic engineering from Hanyang University, Seoul, South Korea, in 2021. He is currently a Postdoctoral Researcher with Hanyang University. His research interests include implantable antennas and systems, biomedical circuits, wearable antennas, MIMO communication, metamaterial, dielectric resonator antennas, reconfigurable antennas, long-range wireless power transfer, and wireless charging of biomedical implants. He received the Silver Prize for the Best Student Paper Awards in Student Paper Contests 2018 and 2019, IEEE Seoul Section. His collaborated paper received the Best Paper Award 2019 by IEEE AP/MTT/EMC Joint Chapter Malaysia. He received the Third Prize for the Best Student Paper Completion 2018 by the Korea Communications Agency (KCA) and the Korean Institute of Electromagnetic Engineering and Science (KIEES).

MUHAMMAD ZADA (Graduate Student Member, IEEE) received the B.Sc. degree in telecommunication engineering from the University of Engineering and Technology, Peshawar, Pakistan, in 2015, and the integrated M.S./Ph.D. degree in electronic engineering from Hanyang University, Seoul, South Korea, in 2023.

He is currently a Postdoctoral Fellow with Hanyang University. He has published over 20 papers in high-quality journals and conference proceedings in the field of telecommunications, electronic, and biomedical engineering. His current research interests include implantable antennas and devices, intra-oral tongue drive systems, wireless power transfer, energy harvesting, smart-textile millimeter-wave antennas, MIMO antennas, wearable sensors and antennas, microwave breast cancer detection, metamaterials, and EBGs.

Dr. Zada has received the Best Student Paper Competition 2018 Award from the Korean Institute of Electromagnetic Engineering and Science (KIEES). He is serving as a Reviewer for IEEE TRANSACTIONS, the *International Journal of RF and Microwave Computer-Aided Engineering* (RFCAD), MDPI journals, and Elsevier journals.

SADIQ ULLAH (Senior Member, IEEE) received the B.Sc. degree in electrical engineering from the University of Engineering and Technology Peshawar, Peshawar, Pakistan, the M.Sc. degree in electrical engineering from the University of Engineering and Technology Taxila, Pakistan, and the Ph.D. degree for his research in the field of design and measurement of metamaterial-based antennas, in 2010. In 2007, he joined the Department of Electronic and Electrical Engineering, Loughborough University, U.K. He was an Assistant Manager (Electronics) in a public sector research and development organization in Islamabad, where his main responsibilities were hardware, software co-design, designing and testing of high precession electronics, and test equipment. He was a Research Associate with Loughborough University, where he researched the propagation effects of rain, snow, ice, fog, and forest in millimeter wave bands. He is currently a Professor and the Head of the Telecommunication Engineering Department, University of Engineering and Technology Mardan, Mardan, Pakistan. His research is published in international conferences and peer-reviewed journals. His research interests include the design and measurement of metasurfaces, metamaterial-based antennas, 5G MIMO antennas, multiband/wideband antenna, SAR, and wearable antennas.

BABAR KAMAL received the B.Sc. degree in electronics engineering from BUITEMS, Quetta, Pakistan, the M.Sc. degree in telecommunication engineering from the University of Engineering and Technology, Peshawar, Pakistan, and the Ph.D. degree in information and communication engineering from Northwestern Polytechnical University (NWPU), China. He is currently a Postdoctoral Fellow with the Center of Intelligent Acoustics and Immersive Communication, School of Marine Science and Technology, NWPU. His research interests include metasurfaces, metamaterials, wearable antennas, multiband/wideband antennas, polarization control devices, and absorbers.

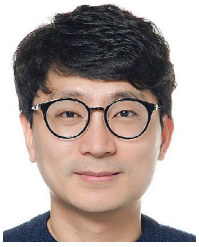

HYOUNGSUK YOO (Senior Member, IEEE) received the B.Sc. degree in electrical engineering from Kyungpook National University, Daegu, South Korea, in 2003, and the M.Sc. and Ph.D. degrees in electrical engineering from the University of Minnesota, Minneapolis, MN, USA, in 2006 and 2009, respectively.

In 2009, he joined the Center for Magnetic Resonance Research, University of Minnesota, as a Postdoctoral Associate. In 2010, he joined Cardiac Rhythm Disease Management, Medtronic, MN, USA, as a Senior EM/MRI Scientist. From 2011 to 2018, he was an Associate Professor with the Department of Biomedical Engineering, School of Electrical Engineering, University of Ulsan, Ulsan, South Korea. He has been the CEO of E2MR, a startup company, since 2017. Since 2018, he has been a Professor with the Department of Biomedical Engineering and the Department of Electronic Engineering, Hanyang University, Seoul, South Korea. His current research interests include electromagnetic theory, numerical methods in electromagnetics, metamaterials, antennas, implantable devices, and magnetic resonance imaging in high-magnetic field systems.

Dr. Yoo received the Third Prize for the Best Student Paper from the 2010 IEEE Microwave Theory and Techniques Society International Microwave Symposium.